

Prediction of activation energy barrier of island diffusion processes using data-driven approaches  
Shree Ram Acharya<sup>1</sup> and Talat S. Rahman<sup>1, 2\*</sup>

<sup>1</sup>Department of Physics, University of Central Florida, Orlando, FL 32816, USA

<sup>2</sup>Donostia International Physics Center, Donostia-San Sebastian, 20018, Spain

We present models for prediction of activation energy barrier of diffusion process of adatom (1-4) islands obtained by using data-driven techniques. A set of easily accessible features, geometric and energetic, that are extracted by analyzing the variation of the energy barriers of a large number of processes on homo-epitaxial metallic systems of Cu, Ni, Pd, and Ag are used along with the activation energy barriers to train and test linear and non-linear statistical models. A multivariate linear regression model trained with energy barriers for Cu, Pd, and Ag systems explains 92% of the variation of energy barriers of the Ni system, whereas the non-linear model using artificial neural network slightly enhances the success to 93%. Next mode of calculation that uses barriers of all four systems in training, predicts barriers of randomly picked processes of those systems with significantly high correlation coefficient: 94.4% in linear regression model and 97.7% in artificial neural network model. Calculated kinetics parameters such as the type of frequently executed processes and effective energy barrier for Ni dimer and trimer diffusion on the Ni(111) surface obtained from KMC simulation using the predicted (data-enabled) energy barriers are in close agreement with those obtained by using energy barriers calculated from interatomic interaction potential.

## I. INTRODUCTION

The development of computational approaches that enable long time simulation of atomic system that reveal rare events responsible for system dynamics and morphological evolution is an ongoing research topic. The kinetic Monte Carlo (KMC) method<sup>1,2</sup> that approximates a system evolution as succession of state-to-state Markov walks dictated by rates of all possible processes is taken as one of the method of choice in such studies. In KMC, the probability to execute a process is proportional to its rate and the time advanced after each process execution depends inversely on the sum of the rates of all possible processes in the system. The rate for atomic diffusion processes on surface follows Arrhenius rate expression from transition state theory<sup>2,3</sup>

$$k_{ij} = r_0 e^{\frac{-E_a}{k_B T}}, \quad (1)$$

where  $k_{ij}$ ,  $r_0$ ,  $E_a$ ,  $k_B$  and  $T$  are the rate of transition from state  $i$  to state  $j$ , an attempt frequency, activation energy barrier of the process, the Boltzmann constant, and the absolute temperature, respectively. The quantity  $E_a$  is the energy difference between the maximum energy in the minimum energy path (MEP) and the energy of the stable initial configuration on which the process in question executes. For a given interatomic interaction, various methods<sup>4-7</sup> are in use to compute the MEP and then an  $E_a$  of a process. Although such a calculation using a semi-empirical interatomic interaction is orders of magnitude faster in comparison to the first principles calculation based on density functional theory, it is still computationally intensive. Not surprisingly, attempts have been made to predict activation energy barriers from other considerations. Such studies can broadly be classified as methods that infer  $E_a$  from other quantities and those that directly predict  $E_a$ . Along the first category, a correlation between the diffusion barrier of atomic or molecular species and their binding energy on transition metal surfaces is

proposed as 12% of the binding energy,<sup>8</sup> the energy of end state and energy difference between the final and initial configurations<sup>9</sup> and <sup>10</sup>, respectively. In chemical reaction studies: Michaelides et al.<sup>11</sup> infers  $E_{as}$  of dissociative reactions in heterogeneous catalysis using enthalpy change, refs. <sup>12-14</sup> infer a linear correlation between the transition state energy and the final state energy in elementary steps by exploring the bond breaking reaction of diatomic molecules on surface catalysts, Jacob et al.<sup>15</sup> showed oxygen p-band center as measure of perovskite compounds catalytic activity. These correlations provide a convenient tool for prediction of barriers which would enable computational screening of catalyst. In the second category, simplified approaches based on the counting of broken and newly formed bonds<sup>16-19</sup> and sophisticated ones based on cluster expansion<sup>20, 21</sup>, genetic programming<sup>22</sup>, and artificial neural network<sup>19, 23-26</sup> for vacancy migration barrier are used.

In island diffusion study, although repeated calculation of barriers of the different possible single-atom, multi-atom, and concerted processes can be avoided by using pattern recognition scheme, for example in the self-learning kinetic Monte Carlo (SLKMC) method<sup>27</sup>, even one time calculation of barriers of those processes for every system is a time consuming task. In this work we use data-driven methods to analyze the variation of the activation energy barriers of a set of systems, for which a large data base has been acquired using SLKMC. We then generate local geometric and energetic descriptors that might serve predictors of these energy barriers for related systems. These descriptors are then used to develop predictive model to efficiently calculate barrier of process of new systems.

In what follows, we explain the computational details including considerations in descriptors generation and basics of models in section II, results including comparison of predicted and calculated barriers in section III, and offer conclusions in section IV.

## II. COMPUTATIONAL DETAILS

### A. Database of energy barriers of diffusion processes

In this study, information about the geometry of island before and after execution of a process and the energy barriers of 844 processes are taken which are collected from our SLKMC study of homo-epitaxial dimer to tetramer adatom island diffusion of Ni, Cu, Ag, and Pd systems. Those barriers of are calculated using drag method with embedded atom method (EAM)<sup>28</sup> interaction in a system consisting an adatom island of interest on 5-layers of substrate each with 256 (16x16) atoms. The details of the method is explained in ref<sup>27, 29</sup>. Out of 844 processes, 168 are of Cu/Cu(111), 191 of Ag/Ag(111), 156 of Pd/Pd(111) and 328 of Ni/Ni(111). The barriers range from 0.003eV to 1.302eV.

### B. Descriptors selection

To choose descriptors, we analyze the variation of barrier of processes executed by the same adatom of an island on different target sites on underlying substrate and different configurations that enables us to guess quantities which are different in those processes as a possible source of the variation of barriers. As source, we consider the initial and final geometry of an island, the local neighborhood on the top substrate layer and some energetic quantities. The selection of descriptors and their sufficiency is very crucial to get high correlation between the predicted barriers using a model and the calculated barriers. The rational used in the identification of descriptors is explained in this section by taking some example processes of Pd island on Pd(111) surface. In the following figures, the adatoms are represented by filled blue circles, bond between them by red lines, executed processes by black lines with arrowhead and substrate by orange lines on which atom exists at each node.

### 1. Number of bonds that change ( $x_1$ )

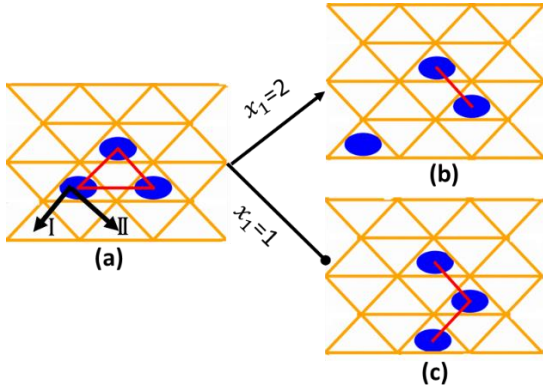


Figure 1. (a) A trimer island with three number of bonds among adatoms on which two among many possible single-atom processes executed by an adatom are shown on which the process I and II generate final structures shown on right with one and two bonds, respectively.

In the trimer island shown in Fig.1, the initial configuration has 3 bonds among adatoms on which the final configuration formed after execution of process I and II in Fig. 1 (a) has 1 and 2 bonds so that the changes on the number of bonds are 2 and 1, respectively. The processes I and II have barrier of 1.147eV and 0.629eV, respectively. The change in the number of bonds before and after execution of a process is taken as descriptor  $x_1$  which has value 2 and 1 for the processes I and II shown in Fig.1. This is not surprising, as it costs energy to break a bond and so the larger the number of broken bonds to be broken requires the higher energy cost.

The frequency distribution of the values of each descriptor in our database is shown along diagonal boxes and the pairwise correlation between descriptors and activation energy barrier is shown on off-diagonal boxes in the scatter plot shown in Fig. 5. The values of Pearson's correlation coefficient for each pair are shown in each off-diagonal boxes. The discussion of the plot follows after discussion of descriptors.

## 2. Shift of island geometric center ( $x_2$ )

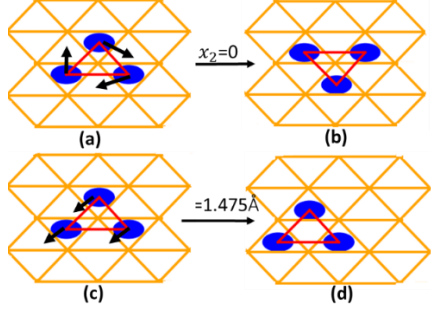


Figure 2. A trimer island in (a) or (c) forms islands in (b) and (d) after executing rotational process (shown in (a)) and translational process (shown in (c)), respectively. The values over line are the shift of geometric center.

For the trimer island shown in Fig. 2(a) or (c), the barriers of the shown processes: rotational from (a) to (b) and translational from (c) to (d) are 0.094eV and 0.151eV, respectively. The change in the value of the descriptor  $x_1$  is zero in both of the processes while the barriers of the processes are different that necessitate additional descriptor. In Fig. 2, we show the variation of the value of the shift of geometric center of the island, which we take as value of descriptor  $x_2$ : 0Å and 1.475Å for the shown rotational and translational processes, respectively.

## 3. A-or B-type process ( $x_3$ )

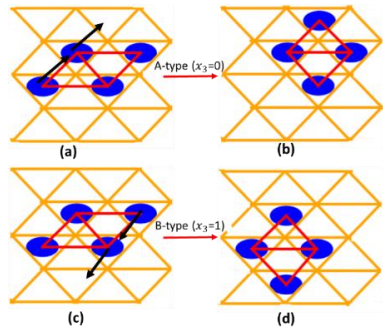


Figure 3. Processes executed by adatoms on (a) (100) micro-facet or A-step, (c) (111) micro-facet or B-step, that are executed on the same island configuration and lead to the same final island configuration shown in (b) or (d).

The edges of an island on fcc(111) surfaces form either (100) micro-facet (called A-step) or (111) micro-facet (called B-step) with the underlying terrace. The two adatoms in tetramer island shown in Fig. 3 (a) with lines with arrowhead attached on them form A-step and remaining two atoms (which are also attached with lines with arrow in Fig. 3(c)) form B-step. Those two processes shown on Fig. 3(a) and (c) start on the same island and transform the island into the same final island configuration shown in Fig. 3(b) or (d). The values of both of the descriptors  $x_1$  and  $x_2$  explained before remain same for both of the processes, however, the barriers of process executed by atoms in A-step (A-type process) is 0.319 eV and that of process executed by atoms in B-step (B-type process) is 0.485eV, a significant variation. So, we introduce a binary descriptor  $x_3$  that takes value 0 if the process is A-type and 1 if it is B-type.

#### 4. Number of diffusing atoms in a process ( $x_4$ )

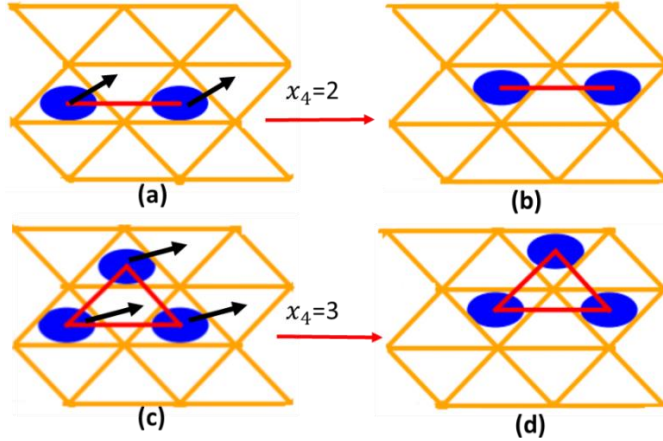


Figure 2. Translational concerted processes of a (a) dimer, and (c) trimer island. The barriers of the processes are 0.113 eV and 0.148 eV, respectively.

For small size of islands, concerted motion of an island is an important contributor to the diffusivity. In Fig. 4, concerted processes in a dimer and a trimer islands are shown for which the value of their activation energy barrier are 0.113eV and 0.155eV, respectively. Since for those

processes, the values of each of the descriptors introduced before have the same value, , we add the number of atoms in the island as an additional descriptor  $x_4$  which takes value 2 and 3 for the processes shown in Fig. 4.

### 5. Binding energy of adatom island with substrate ( $x_5$ )

As shown in ref. <sup>30</sup>, the energy barriers of diffusion processes of Ni island on Ni(111) are in general larger than those of the corresponding processes of Cu islands on the same Ni(111) substrate. Similar trend also holds when comparing Ag and Pd systems, as can be seen in Table I in which we have summarized the energy barrier of some representative processes for several homo-epitaxial and hetero-epitaxial systems. Although our training data contains only for homo-epitaxial system, we include hetero-epitaxial systems to show the general trend.

Table I. Diffusion barriers of some selected single-atom (S), multi-atom (M), and concerted (C) processes of adatom islands on several homo-epitaxial and hetero-epitaxial islands on fcc(111) system.

Island Size	Energy barrier(eV)							
	Cu/Ni	Ni/Ni	Cu/Cu	Ni/Cu	Pd/Ag	Ag/Ag	Pd/Pd	Ag/Pd
1	0.052	0.059	0.030	0.032	0.054	0.059	0.037	0.055
2(S)	0.029	0.034	0.013	0.028	0.033	0.055	0.026	0.065
2(C)	0.059	0.066	0.019	0.021	0.066	0.098	0.043	0.065
3(C)	0.152	0.187	0.103	0.132	0.241	0.176	0.168	0.176
4(M)	0.191	0.271	0.194	0.282	0.355	0.244	0.320	0.221

Table II. Size-dependent adatom island binding energy on several homo-epitaxial and hetero-epitaxial islands on fcc(111) system.

Island Size	Island binding energy (eV)							
	Cu/Ni	Ni/Ni	Cu/Cu	Ni/Cu	Pd/Ag	Ag/Ag	Pd/Pd	Ag/Pd
2	-3.29	-3.28	-3.04	-3.04	-3.94	-1.96	-3.89	-2.93
3	-4.24	-4.18	-3.89	-3.83	-5.04	-2.49	-5.07	-3.84
4	-5.37	-5.29	-4.93	-4.86	-6.33	-3.16	-6.40	-4.93

By comparing the energy barriers in the first four columns in Table I, one can see that those for the diffusion of Cu islands on either Cu(111) (Cu/Cu in Table I) or Ni(111) are lower than those of the corresponding Ni islands on the same substrate. A similar relation holds for Ag islands having relatively higher barriers in most cases than Pd islands on both Pd(111) and Ag(111) as presented in last four columns in the Table I. To obtain qualitative understanding of the above trends, we present in Table II the binding energy (B.E.) of adatom islands on respective surface mentioned in Table I calculated using

$$\text{B.E.} = E_{\text{island+subs.}} - E_{\text{island}} - E_{\text{subs.}}, \quad (2)$$

where  $E_{\text{island+subs.}}$ ,  $E_{\text{island}}$ ,  $E_{\text{subs.}}$  are the energy of a system containing the adatom island on the substrate, the isolated island, and the isolated substrate, respectively. One can see from Table II that B.E. of the Cu islands on Ni(111) are stronger than that of Ni islands on the same surface, while that of Pd islands are stronger than that of Ag islands on the same substrate. Based on the consistent relation, we consider the binding energy of the adatom island as descriptor  $x_5$ .

#### *6. Lateral interaction energy among adatoms ( $x_6$ )*

In an earlier work<sup>30</sup>, we had emphasized the role of lateral interaction to understand the relatively smaller barriers of the diffusion processes of Cu adatom islands than that of Ni on the Ni(111) substrate. The slight difference in the binding energy of Cu and Ni islands on Ni(111) (first 2 columns of Table II) also indicates that several factors beyond binding energy are responsible for the noticeable differences in diffusion barriers for otherwise similar processes of the Cu and Ni islands on Ni(111). To examine the role of lateral interactions in a general manner we turn here to a comparison of some frequently-executed multi-atom and concerted processes of islands of different sizes for four different systems on in Table III which has difference in kinetics

(see ref. <sup>29</sup> ) appears as consequence of difference in barriers of their multi-atom and concerted processes.

Table III. Comparison of barriers of concerted and multi-atom processes for the same adatom island configuration in homo and hetero-epitaxial systems.

Island Size	Energy barrier (eV)							
	Pd/Pd		Ag/Ag		Cu/Ni		Ni/Cu	
	Concerted	Multi-Atom	Concerted	Multi-Atom	Concerted	Multi-Atom	Concerted	Multi-Atom
4	0.186	0.324	0.190	0.246	0.182	0.205	0.157	0.303
5	0.277	0.345	0.281	0.254	0.235	0.196	0.220	0.313
6	0.284	0.643	0.299	0.551	0.290	0.580	0.222	0.731
7	0.327	0.418	0.417	0.319	0.460	0.318	0.431	0.277
8	0.416	0.665	0.401	0.469	0.378	0.477	0.356	0.611

In Table III, one can make two observations: there is a noticeable difference in the barriers of concerted and the multi-atom processes for the same island configuration and that the magnitude of the difference is system dependent. We find the order to be Ni/Cu, Pd/Pd, Cu/Ni, and Ag/Ag i.e, the difference is in general large in Ni/Cu and Pd/Pd systems. Such a difference might be understood from the interatomic interaction among adatoms. One quantitative measure of such is the lateral interaction amongst the adatoms in the island which is defined by

$$E_{LI} = E_{island+sub.} - nE_{mono+sub.} + (n - 1)E_{sub.} \quad (3)$$

where  $E_{island+sub.}$ ,  $E_{mono+sub.}$ , and  $E_{sub.}$  are the total energy of the system with the island on the substrate, a monomer on the substrate, and that of an isolated substrate, respectively. The calculated values of  $E_{LI}$  for four different systems whose energy barriers are in Table III are presented in Table IV. Note again that although our training data is for homo-epitaxial systems, we have brought hetero-epitaxial systems to clarify the ideas.

Table IV. Lateral interaction among adatoms of islands on the fcc(111) substrate for the configurations relevant to processes in Table III.

Island Size	Lateral interaction energy (eV)			
	Pd/Pd	Ag/Ag	Cu/Ni	Ni/Cu
2	-0.54	-0.32	-0.39	-0.54
3	-1.49	-0.89	-1.09	-1.44
4	-2.42	-1.42	-1.89	-2.30
5	-3.29	-1.94	-2.58	-3.12
6	-4.2	-2.46	-3.28	-3.96
7	-5.45	-3.19	-4.26	-5.13
8	-6.33	-3.69	-4.94	-5.94

In Table IV, one can see that the Pd/Pd and Ni/Cu systems which have the relatively large difference between barriers of concerted and multi-atom processes, with low barriers of concerted processes compared to their multi-atom process barriers, have strong lateral interactions among adatoms whereas the Ag/Ag and Cu/Ni systems have relatively weak interaction among adatoms. Due to role of lateral interaction to get understanding about variation of barriers of concerted and multi-atom on different systems, we consider it as descriptor  $x_6$ .

The distribution of values of those six descriptors, correlation between them and with the activation energy barrier is shown using scatter matrix plot in Fig. 5.

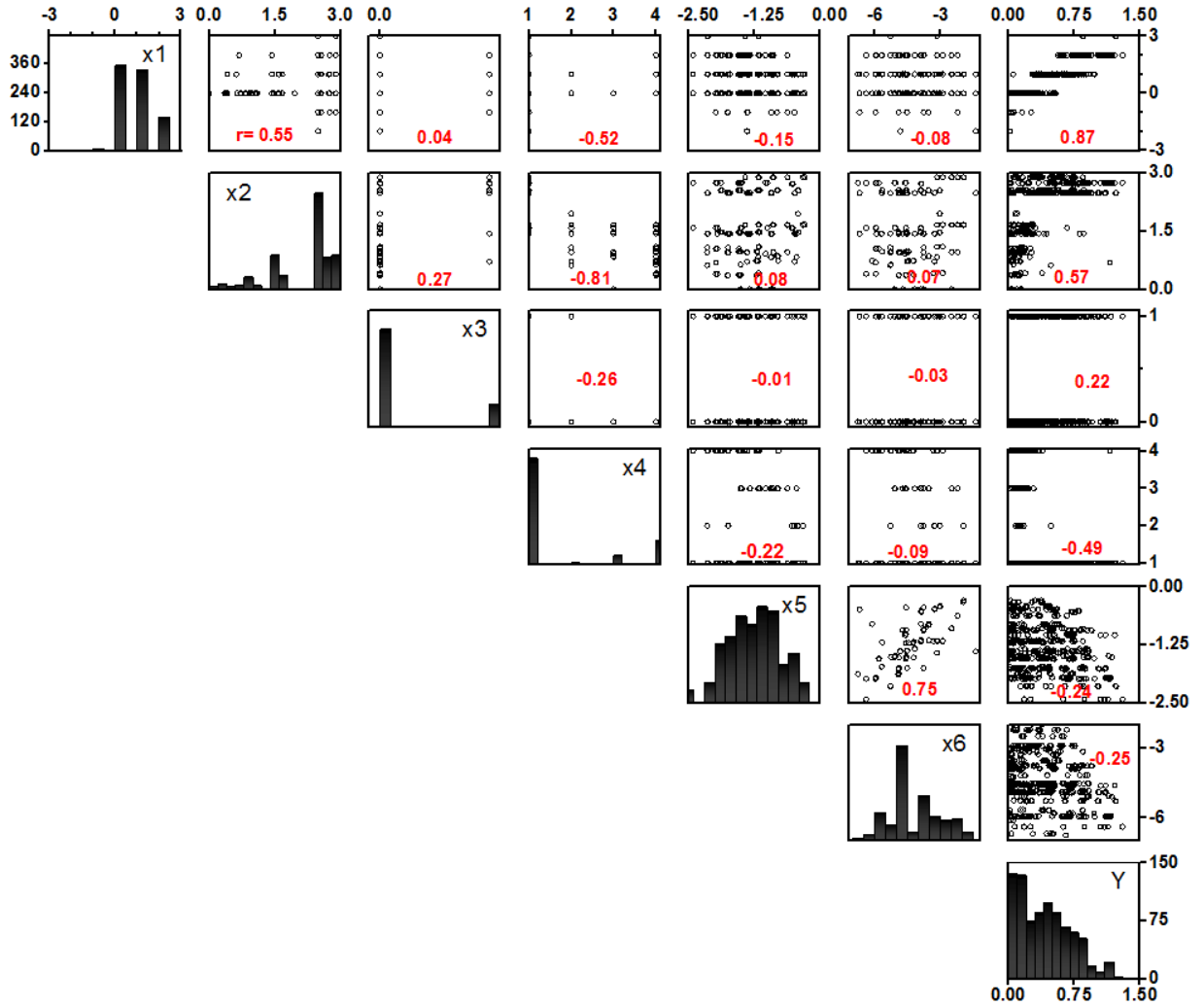


Figure 5. A scatter matrix plot that shows the frequency distribution of the variables along diagonal boxes and the pairwise correlation between variables on off-diagonal boxes. The values of Pearson's correlation coefficient for each pair are shown in each off-diagonal boxes.

From the frequency distribution of descriptor  $x_1$  (number of bonds change) in our database (see the top left box in Fig. 5), one can see that descriptor  $x_1$  has positively skewed distribution on which the number of instances with bond change of -2, -1, 0, 1, 2, and 3 are 2, 10, 352, 335, 141 and 4, respectively. So, there are large number of processes in our database in which either the number of bonds does not change or decrease by 1 or 2 after executing it. Comparison of the value

of the correlation coefficient between the descriptor  $x_1$  and other descriptors as shown on five successive boxes on the top row indicate that  $x_1$  has relatively strong positive correlation with descriptor  $x_2$  (shift of island geometric center) which means that in number of instances where the number of bonds change, the shift of island geometric center increases and negative correlation with  $x_4$  (number of diffusion atoms) indicate in instances with the small change in the number of bonds with increase number of atoms involved in diffusion, for e.g., concerted process having lower barrier than small number of atom involving processes. Lack of definite tendency between  $x_1$  with descriptor  $x_3$  (A- or B-type process), descriptor  $x_5$  (island binding energy on substrate) and  $x_6$  (lateral interaction energy among adatoms) indicates they are independent. The descriptor  $x_1$  has high positive correlation with activation energy barrier with value of Pearson's coefficient being 0.87, the highest among the selected descriptors which reflects that processes with relatively large number of bonds change have relatively higher barrier.

The descriptor  $x_2$  has values that distribute from 0 to 3 Å which possess strong negative correlation with values of descriptor  $x_4$  which reflects the fact that the most of single atom processes are long jump with high value of distance travelled whereas the multi-atom or concerted are short jump and give even small value of the distance travelled when distance is divided by the number of atoms involved in process. The descriptor  $x_2$  has high positive correlation with activation energy barrier with value of Pearson's coefficient being 0.57, which reflects the fact that long jump processes for e.g., detachment single atom processes that change the distance more have relatively higher barrier.

The distribution of values of descriptor  $x_3$  show that there are large number of A-type processes in our database. The descriptor  $x_3$  has small negative correlation with  $x_4$  indicates that

in our database A- type process has more number of diffusion atoms while B-type process has relatively less number of diffusion atoms. The descriptor has positive correlation with value 0.22 with activation energy barrier indicating B-type processes have relatively high barrier. The descriptor has negligible relation with other descriptors.

The distribution of values of descriptor  $x_4$  includes that there are large number of single atom processes. The negative correlation with binding energy indicates that there are the single atom processes or less number of atom moving processes most in systems with higher binding energy with substrate. The negative correlation with activation energy barrier reflects the relatively small value of barriers of non-detaching multi-atom or concerted processes in comparison to that of many detaching single atom processes in our database.

The values of descriptor  $x_5$  are almost normally distributed and has strong correlation with value 0.75 with descriptor  $x_6$  indicating that the system with larger binding energy with substrate also has larger lateral interaction. Such a tendency can also be seen from Table I and Table IV in which Pd/Pd system has both quantity largest and Ag/Ag has both the lowest but it does not hold in Cu/Ni and Ni/Cu system.

The descriptor  $x_6$  (lateral interaction energy) has values in range -7eV to 1 eV and has negative correlation with the barrier of processes. The decrease of barrier of concerted processes in comparison to that of multi-atom process in system with larger lateral interaction is already discussed when describing descriptor  $x_6$ .

The values of these six descriptors and the barrier of processes are used in a data-enabled model to predict the diffusion barriers.

## C. Predictive models

### 1. Multivariate linear regression (MLR)

As an initial step, a predictive model based on multivariate linear regression technique which assumes independent variables linearly contribute to the dependent variable is tested whose mathematical form is

$$y_i = \beta_0 + \sum_{j=1}^6 \beta_j x_j + \epsilon_i, \quad (4)$$

where  $y_i$  represents the predicted value of dependent variable ( $E_a$  of a diffusion process in this study) on the  $i^{th}$  instance ( $i$  has value 844 when all data is used to develop model in this study) and  $x_j$  is the value of  $j^{th}$  independent variables, ( $j=1, 2, \dots, 6$ ) on the same instance. The parameters  $\beta_0$  and  $\beta_j$ s represent an intercept and the predictor  $x_j$ 's slope, respectively and  $\epsilon_i$  represents error term on  $i^{th}$  instance. Taking error function as the sum of square of errors and applying the condition of its minimization with respect to parameter  $\beta$ s, one can get a matrix of values of fitting parameters  $\beta$ s using

$$\beta = (X^T X)^{-1} X^T Y, \quad (5)$$

where  $X$  refers a matrix formed with values of 6 descriptors along column and training samples as rows,  $T$  refers the transpose operation of matrix and  $Y$  is a column matrix formed by calculated activation energy barriers,  $c_i$ . The Pearson's correlation coefficient ( $R$ ) between  $c_i$ s and  $y_i$ s is used for quantitative measure of the predictive capacity of the model which is calculated using

$$R = \frac{N \sum_i y_i c_i - \sum_i y_i \sum_i c_i}{\sqrt{[N \sum_i y_i^2 - (\sum_i y_i)^2][N \sum_i c_i^2 - (\sum_i c_i)^2]}}, \quad (6)$$

where  $N$  represents the sample size used to predict.

## 2. Non-linear model using Artificial Neural Network (ANN)

In this study, the possibility of a non-linear dependence between independent and dependent variables is modeled by using artificial neural network (ANN)<sup>31</sup> approach as implemented in MATLAB software. Because of the ability of ANN to identify underlying highly complex and non-linear relationships on input-output data, it become a method of our choice for data fitting purposes. The structural organization of the ANN used in this study consists of input with 6 nodes corresponding to 6 input features ( $x_j$ s), 2 hidden layers containing 10 nodes each with sigmoid and linear transfer function for 1<sup>st</sup> and 2<sup>nd</sup> hidden layers respectively, and output layer. Following the fitting mechanism of an ANN, the mathematical expression for the value on k<sup>th</sup> node (k=1, 2, ..,10) in 1<sup>st</sup> hidden layer ( $x_k^1$ ) is given by

$$f\{\sum_{j=1}^6(w_{kj}^1x_j + b_k^1)\} = x_k^1,$$

where the superscript refers hidden layer number,  $w_{kj}^1$  and  $b_k^1$  are the weight and bias at node k in 1<sup>st</sup> hidden layer for each instances of input  $x_j$  in input layer and f is transfer function (sigmoid in this study). The value on p<sup>th</sup> node (p=1,2, ..,10) in 2<sup>nd</sup> hidden layer ( $x_p^2$ ) is given by

$$f\{\sum_{k=1}^{10}(w_{pk}^2x_k^1 + b_p^2)\} = x_p^2,$$

where the second transfer function is linear function in this study. The output ( $y_i$ ) which gives the predicted barrier is given by

$$y_i = f\{\sum_{p=1}^{10}(w_{ip}x_p^2 + b_i)\}.(7)$$

The mean square error (MSE) is taken as error function which is calculated as

$$\text{Error function} = \text{MSE} = \sum_{i=1}^N \frac{(y_i - c_i)^2}{N},$$

where  $c_i$  refers to the calculated energy barrier or target value assigned at the beginning of fitting and N is the number of training samples. During the training process, the weights and biases are

adjusted to optimize the function that converts the neural network training problem into an optimization problem. Levenberg-Marquardt\_algorithm<sup>32, 33</sup> is used as optimizer in which the current weight and bias vector ( $v_k$ ) is updated to vector  $v_{k+1}$  following

$$v_{k+1} = v_k - (JJ + I * \mu)J_e,$$

where  $I$  is an identity matrix,  $\mu$  is a training rate parameter which influences the rate of weight and bias adjustment and  $JJ = (J_F)^T(J_F)$  for  $J_F$  being the Jacobian of performance function with respect to weights and biases.. In this study, the initial weight and biases are randomly selected and the initial value of the learning rate parameter  $\mu$  is taken as 0.001 which is increased by a factor of 10 until the updated  $x_{k+1}$  results in a reduced performance after which  $\mu$  is decreased by a factor of 0.1. During training, the network performance in the validation vectors is checked every epoch and if it increases or remains constant in the current step for 6 additional epochs in a row or the performance error is 0 or the gradient of the error is less than  $10^{-7}$ , the calculation is terminated.

### III. RESULTS

In this section, we present results of predicted diffusion barriers obtained from using multivariate linear regression and neural network techniques.

In the first set of calculation, a multivariate linear model is formed by taking each atomic system separately. The value of  $R^2$  obtained using Equation (6) and the expansion coefficients as obtained by using equation (5) are presented in Table V. A model formed by taking all 844 samples of the input-output pair is used to predict values of Ni barriers in which case the value of  $R^2$  between the calculated and the predicted values is 0.893 ( $R = 0.944$ ). The high value of  $R^2$  indicates that the 6 descriptors used in this study are sufficient to explain the variability of output variable (activation energy barrier) and can predict barrier reliably.

Table V. Calculated coefficients in the linear predictive equation of activation energy barrier using 6 descriptors and value of  $R^2$  for models.

System	Sample Size	Coefficients							$R^2$	
		$\beta_1$	$\beta_2$	$\beta_3$	$\beta_4$	$\beta_5$	$\beta_6$	Intercept		
Cu	168	0.327	-0.09	0.098	0.062	0.002	0.029	-0.094	0.96	
Ag	191	0.232	-0.057	0.107	0.055	-0.240	0.223	0.274	0.904	
Pd	157	0.472	0.119	0.203	0.057	0.048	-0.007	-0.157	0.95	
Ni	328	0.323	0.111	0.132	0.056	-0.019	0.016	-0.63	0.922	
CuAgPdNi	844	0.314	0.085	0.119	0.036	0.041	-0.058	-0.277	0.841	
Ni using CuAgPdNi	328	0.898							0.0303	0.893
CuAgPd	516	0.318	0.095	0.109	0.047	0.122	-0.094	-0.365	0.814	
Ni using CuAgPd	328	0.889							0.036	0.85

As a second scenario, we use the dataset of Cu, Ag, and Pd systems that contains 516 samples to develop a model and test its predictive capacity for the Ni system. The value of  $R^2$  in this case comes out to be 0.85 ( $R= 0.921$ ). The calculated and predicted activation energy barriers of the Ni system in the first and second scenario are plotted in Fig. 6(a) & (b), respectively. The blue continuous line represents an ideal case.

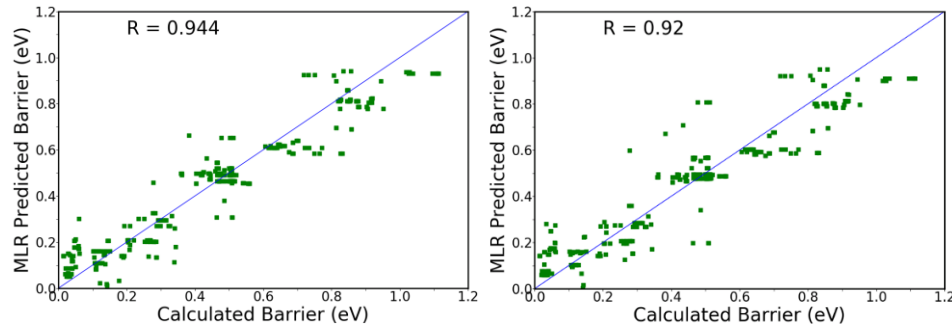


Figure 3. Predicted vs. calculated barriers of processes for Ni islands on the Ni(111) surface, (a) when some Ni samples are used to train of linear model and (b) Ni samples are not used to train the model.

When using neural network, training, validation, and testing data sets are randomly selected from input data in 70%, 15% and 15%, respectively. The value of correlation coefficients between calculated and predicted barriers are presented in Table VI.

Table VI. Values of correlation coefficients in the training, validation, and testing dataset of diffusion barriers using the neural network.

System	Sample Size	Correlation Coefficient (R)		
		Training	Validation	Testing
Cu	168	0.99	0.98	0.98
Ag	191	0.99	0.99	0.99
Pd	157	0.99	0.97	0.98
Ni	328	0.99	0.98	0.99
CuAgPdNi	844	0.97	0.97	0.97

The plots of the predicted vs. computed values of barriers of processes for training, validation, and testing data are shown in Fig. 7(a), (b), and (c) respectively. The high value of correlation coefficient has demonstrated that artificial neural network model is good for predicting activation energy barriers.

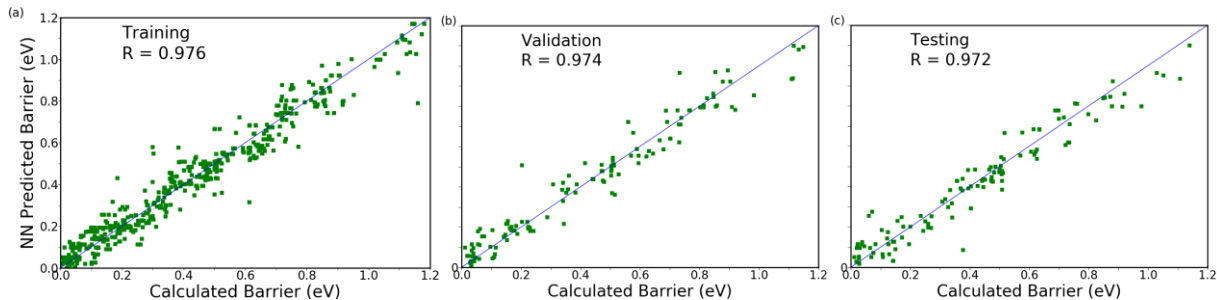


Figure 4. Calculated vs. predicted barriers of different processes of an island diffusion on the fcc(111) surface using a neural network; (a), (b), and (c) show plots for training, validation, and testing samples, respectively.

To test the generality of the model, we predict the activation energy barriers of processes for the Ni excluding the barriers of the system in the training and validation process. A plot of the predicted vs calculated barriers is shown in Fig. 8 and a histogram plot of the error of predictions is shown in Fig. 9.

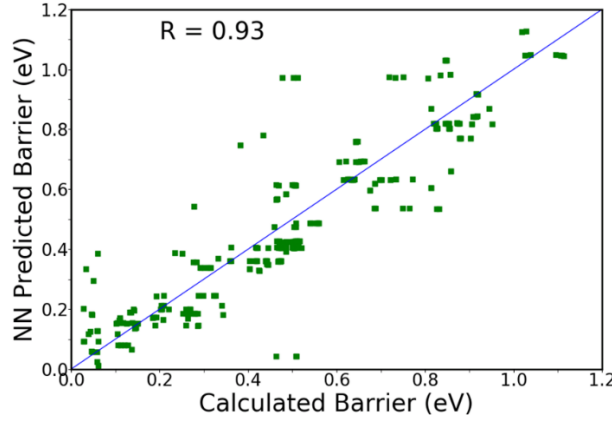


Figure 8. Calculated vs. predicted barriers of different processes of Ni island diffusion on the Ni(111) surface using a neural network model without using Ni barriers in training and validation process.

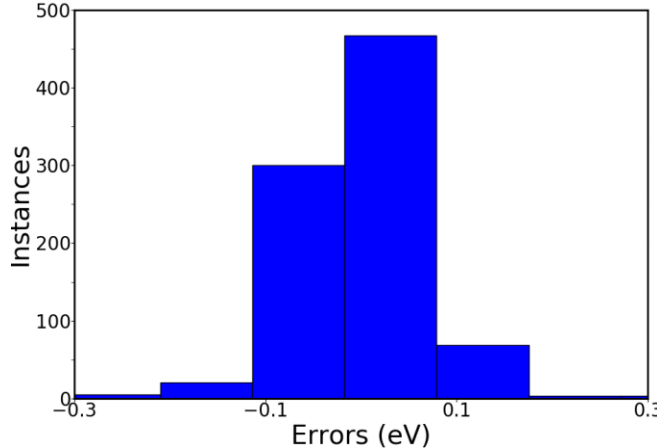


Figure 9. Error histogram of prediction of barriers of Ni/Ni(111) processes using a neural network testing process without using Ni barriers in training and validation process.

From Fig. 9, one can see that there are large number of instances where the error lies in

few meV of the calculated values and the instances with increasing error magnitude decrease with increase in error value.

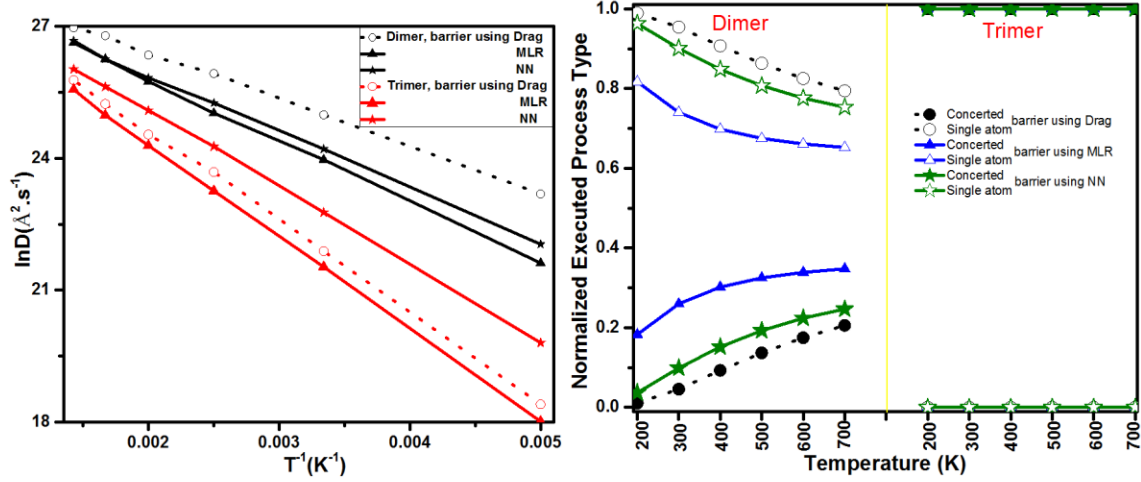


Figure 10. (a) Arrhenius plot, (b) normalized type of executed processes obtained from KMC simulation of the Ni dimer and trimer diffusion processes on the Ni(111) surface using barriers from drag method from EAM interaction and from the trained neural network model.

The predicted barriers are then used to explore the diffusion properties of the island using the kinetic Monte Carlo method. The Arrhenius plot and the normalized type of executed processes (single, multi-atom, concerted) in the simulation of dimer and trimer island diffusion in the temperature range 200K to 600K are presented in Fig. 10.

The close agreement of the quantities plotted in Fig. 10 imply that the predictive approach can be used to find reliable diffusion characteristics of islands of any size of any element in the set of metallic systems considered here, with a significant gain in computational time.

## IV. CONCLUSIONS

We have identified descriptors that when applied in multivariate linear regression and non-linear model using neural network data-driven approaches enables ultrafast prediction of activation energy barriers for metallic island diffusion processes with high accuracy. The accurate prediction of kinetics of new system using the barriers from the models imply that such models can be used in tools for multi-scale modeling of thin film growth and morphological evolution of metallic systems.

## ACKNOWLEDGMENTS

We would like to acknowledge the computational resources provided by the STOKES facility at the University of Central Florida. We thank Duy Le and Mikko Hakala for suggestions for improvements of the manuscript. We are pleased to acknowledge NSF for partial support under grant DMR-1710306.

## REFERENCES

1. A.B. Bortz, M.H. Kalos and J.L. Lebowitz: A new algorithm for Monte Carlo simulation of Ising spin systems. *Journal of Computational Physics* **17**, 10 (1975).
2. A.F. Voter: Classically exact overlayer dynamics: Diffusion of rhodium clusters on Rh (100). *Physical review B* **34**, 6819 (1986).
3. G.H. Vineyard: Frequency factors and isotope effects in solid state rate processes. *Journal of Physics and Chemistry of Solids* **3**, 121 (1957).
4. G. Henkelman and H. Jónsson: A dimer method for finding saddle points on high dimensional potential surfaces using only first derivatives. *The Journal of chemical physics* **111**, 7010 (1999).
5. G. Henkelman, B.P. Uberuaga and H. Jónsson: A climbing image nudged elastic band method for finding saddle points and minimum energy paths. *The Journal of chemical physics* **113**, 9901 (2000).
6. G. Henkelman and H. Jónsson: Improved tangent estimate in the nudged elastic band method for finding minimum energy paths and saddle points. *The Journal of chemical physics* **113**, 9978 (2000).

7. M.J. Dewar, E.F. Healy and J.J. Stewart: Location of transition states in reaction mechanisms. *Journal of the Chemical Society, Faraday Transactions 2: Molecular and Chemical Physics* **80**, 227 (1984).
8. A.U. Nilekar, J. Greeley and M. Mavrikakis: A Simple Rule of Thumb for Diffusion on Transition-Metal Surfaces. *Angewandte Chemie International Edition* **45**, 7046 (2006).
9. H. Kang and W. Weinberg: Dynamic Monte Carlo with a proper energy barrier: Surface diffusion and two-dimensional domain ordering. *The Journal of Chemical Physics* **90**, 2824 (1989).
10. R. Kutner, K. Binder and K. Kehr: Diffusion in concentrated lattice gases. II. Particles with attractive nearest-neighbor interaction on three-dimensional lattices. *Physical Review B* **26**, 2967 (1982).
11. A. Michaelides, Z.-P. Liu, C. Zhang, A. Alavi, D.A. King and P. Hu: Identification of general linear relationships between activation energies and enthalpy changes for dissociation reactions at surfaces. *Journal of the American Chemical Society* **125**, 3704 (2003).
12. Y. Xu, A.V. Ruban and M. Mavrikakis: Adsorption and dissociation of O<sub>2</sub> on Pt–Co and Pt–Fe alloys. *Journal of the American Chemical Society* **126**, 4717 (2004).
13. J.K. Nørskov, T. Bligaard, A. Logadottir, S. Bahn, L.B. Hansen, M. Bollinger, H. Bengaard, B. Hammer, Z. Sljivancanin and M. Mavrikakis: Universality in heterogeneous catalysis. *Journal of Catalysis* **209**, 275 (2002).
14. J. Greeley and M. Mavrikakis: Alloy catalysts designed from first principles. *Nature materials* **3**, 810 (2004).
15. R. Jacobs, J. Hwang, Y. Shao-Horn and D. Morgan: Assessing correlations of perovskite catalytic performance with electronic structure descriptors. *Chemistry of Materials* (2019).
16. Y. Bouar and F. Soisson: Kinetic pathways from embedded-atom-method potentials: Influence of the activation barriers. *Physical Review B* **65** (2002).
17. C. Mottet, R. Ferrando, F. Hontinfinde and A. Levi: A Monte Carlo simulation of submonolayer homoepitaxial growth on Ag (110) and Cu (110). *Surface science* **417**, 220 (1998).
18. M.I. Larsson: Kinetic monte carlo simulations of adatom island decay on cu (111). *Physical Review B* **64**, 115428 (2001).
19. F. Soisson, C. Becquart, N. Castin, C. Domain, L. Malerba and E. Vincent: Atomistic Kinetic Monte Carlo studies of microchemical evolutions driven by diffusion processes under irradiation. *Journal of Nuclear Materials* **406**, 55 (2010).
20. S. Verma, T. Rehman and A. Chatterjee: A cluster expansion model for rate constants of surface diffusion processes on Ag, Al, Cu, Ni, Pd and Pt (100) surfaces. *Surface Science* **613**, 114 (2013).
21. A. Van der Ven and G. Ceder: Vacancies in ordered and disordered binary alloys treated with the cluster expansion. *Physical Review B* **71**, 054102 (2005).
22. K. Sastry, D. Johnson, D. Goldberg and P. Bellon: Genetic programming for multimescale modeling. *Physical Review B* **72** (2005).
23. N. Castin, R. Pinheiro Domingos and L. Malerba: Use of computational intelligence for the prediction of vacancy migration energies in atomistic kinetic monte carlo simulations. *International Journal of Computational Intelligence Systems* **1**, 340 (2008).
24. L. Messina, N. Castin, C. Domain and P. Olsson: Introducing ab initio based neural networks for transition-rate prediction in kinetic Monte Carlo simulations. *Physical Review B* **95**, 064112 (2017).
25. N. Castin, M.I. Pascuet and L. Malerba: Modeling the first stages of Cu precipitation in  $\alpha$ -Fe using a hybrid atomistic kinetic Monte Carlo approach. *The Journal of chemical physics* **135**, 064502 (2011).

26. N. Castin and L. Mallerba: Calculation of proper energy barriers for atomistic kinetic Monte Carlo simulations on rigid lattice with chemical and strain field long-range effects using artificial neural networks. *The Journal of chemical physics* **132**, 074507 (2010).
27. O. Trushin, A. Karim, A. Kara and T. Rahman: Self-learning kinetic Monte Carlo method: Application to Cu(111). *Physical Review B* **72** (2005).
28. S. Foiles, M. Baskes and M. Daw: Embedded-atom-method functions for the fcc metals Cu, Ag, Au, Ni, Pd, Pt, and their alloys. *Physical Review B* **33**, 7983 (1986).
29. S.R. Acharya and T.S. Rahman: Toward multiscale modeling of thin-film growth processes using SLKMC. *Journal of Materials Research* **33**, 709 (2018).
30. S.R. Acharya, S.I. Shah and T.S. Rahman: Diffusion of small Cu islands on the Ni (111) surface: A self-learning kinetic Monte Carlo study. *Surface Science* **662**, 42 (2017).
31. W.S. McCulloch and W. Pitts: A logical calculus of the ideas immanent in nervous activity. *The bulletin of mathematical biophysics* **5**, 115 (1943).
32. D.W. Marquardt: An algorithm for least-squares estimation of nonlinear parameters. *Journal of the society for Industrial and Applied Mathematics* **11**, 431 (1963).
33. M.T. Hagan and M.B. Menhaj: Training feedforward networks with the Marquardt algorithm. *IEEE transactions on Neural Networks* **5**, 989 (1994).